AGB stars in the cosmic matter cycle

https://doi.org/10.1017/S1743921318007184 Published online by Cambridge University Press

Why Galaxies Care About AGB Stars:
A Continuing Challenge through Cosmic Time
Proceedings IAU Symposium No. 343, 2019
F. Kerschbaum, M. Groenewegen & H. Olofsson, eds.

doi:10.1017/S1743921318007184

The role of AGB stars in Galactic and cosmic chemical enrichment

Chiaki Kobayashi, Christopher J. Haynes and Fiorenzo Vincenzo

Centre for Astrophysics Research, University of Hertfordshire,
College Lane, Hatfield, UK
email: c.kobayashi@herts.ac.uk

Abstract. The role of asymptotic giant branch (AGB) stars in chemical enrichment is significant for producing ^{12,13}C, ^{14}N, F, ^{25,26}Mg, ^{17}O and slow neutron-capture process (s-process) elements. The contribution from super-AGB stars is negligible in classical, one-zone chemical evolution models, but the mass ranges can be constrained through the contribution from electron-capture supernovae and possibly hybrid C+O+Ne white dwarfs, if they explode as Type Iax supernovae. In addition to the recent s-process yields of AGB stars, we include various sites for rapid neutron-capture processes (r-processes) in our chemodynamical simulations of a Milky Way type galaxy. We find that neither electron-capture supernovae or neutrino-driven winds are able to adequately produce heavy neutron-capture elements such as Eu in quantities to match observations. Both neutron-star mergers (NSMs) and magneto-rotational supernovae (MRSNe) are able to produce these elements in sufficient quantities. Using the distribution in [Eu/(Fe, α)]–[Fe/H], we predict that NSMs alone are unable to explain the observed Eu abundances, but may be able to together with MRSNe. In order to discuss the role of long-lifetime sources such as NSMs and AGB stars at the early stages of galaxy formation, it is necessary to use a model that can treat inhomogeneous chemical enrichment, such as in our chemodynamical simulations. In our cosmological, chemodynamical simulations, we succeed in reproducing the observed N/O-O/H relations both for global properties of galaxies and for local inter-stellar medium within galaxies, without rotation of stars. We also predict the evolution of CNO abundances of disk galaxies, from which it will be possible to constrain the star formation histories.

Keywords. binaries: general, Galaxy: abundances, galaxies: abundances, hydrodynamics, stars: abundances, stars: AGB and post-AGB, stars: neutron, supernovae: general

1. Introduction

Elemental abundances in the Milky Way Galaxy provide stringent constraints on stellar astrophysics as well as on the formation and evolutionary histories of the Milky Way Galaxy. Elements heavier than helium are synthesized in stars and ejected at their deaths. The next generation of stars forms from gas clouds that include heavy elements from the previous generations. Therefore, stars in the present-day galaxy are fossils that retain the information on the properties of stars in the past. From the elemental abundances of the present-day stars, it is possible to disentangle the star formation history of the galaxy. This approach is called the galactic archaeology. This approach can be applied not only to our Milky Way Galaxy but also to other galaxies (e.g., Kobayashi 2016).

Thanks to the collaboration between nuclear physics and astrophysics, we now have good understanding of the origin of elements in the Universe (e.g., Nomoto *et al.* 2013, hereafter N13). Because of the nature of the triple α reaction, elements heavier with

$A \geqslant 12$ are produced not during the Big Bang, but are instead formed inside stars. Roughly half of the light elements such as C, N and F are produced by low- and intermediate-mass stars ($\sim 0.8-8M_{\odot}$ depending on metallicity) at their asymptotic giant branch (AGB) phase (Kobayashi *et al.* 2011b, hereafter K11). Isotopes such as ^{13}C, ^{17}O, and ^{25,26}Mg are also enhanced by AGB stars, and thus the isotopic ratios can also be used for galactic archaeology (Carlos *et al.* 2018). The α-elements (O, Mg, Si, S, and Ca) are mostly produced in massive stars before being ejected by core-collapse (Type II, Ib, and Ic) supernovae (SNe II, e.g., Kobayashi *et al.* 2006). The production of some elements such as F, K, Sc, and V are increased by neutrino processes in core-collapse supernovae (Kobayashi *et al.* 2011a). Conversely, half of iron-peak elements (Cr, Mn, Fe, Ni, Co, Cu, and Zn) are produced by Type Ia Supernovae (SNe Ia), which are the explosions of C+O white dwarfs (WDs) in binary systems (e.g., Kobayashi & Nomoto 2009). The production of odd-Z elements (Na, Al, P, ... and Cu) depends on the metallicity of the progenitor, as it needs the surplus of neutrons in ^{22}Ne, which is transformed during He-burning from ^{14}N produced in the CNO cycle. The production of minor isotopes (^{13}C, ^{17,18}O, ^{25,26}Mg, ...) also depends on the metallicity.

2. Galactic Chemical Evolution

In Kobayashi, Karakas & Lugaro (2018), we update our galactic chemical evolution (GCE) models in order to match the most recent observations of stars in the solar neighborhood as well as the solar abundance. The basic equations of chemical evolution are described in Kobayashi, Tsujimoto & Nomoto (2000). The code follows the time evolution of elemental and isotopic abundances in a system where the interstellar medium (ISM) is instantaneously well mixed (and thus it is called a one-zone model). No instantaneous recycling approximation is adopted and the chemical enrichment sources with long time-delays are properly included. We adopt the Kroupa initial mass function at $0.01M_{\odot} \leqslant m \leqslant 50M_{\odot}$. The parameters for the star formation history of the system are determined to match the observed metallicity distribution function. The nucleosynthesis yields are taken from K11 for supernovae, and from Karakas & Lugaro (2016) for the slow neutron-capture process (s-process).

The fate of stars with initial masses between about $8-10M_{\odot}$ (at $Z = 0.02$) is uncertain and very interesting, although these contributions were not included in K11. The upper limit of AGB stars, $M_{\rm up,C}$, is defined as the minimum mass for carbon ignition, and is estimated to be larger at high metallicity, and also at low metallicity than at $Z \sim 10^{-4}$. Just above $M_{\rm up,C}$, neutrino cooling and contraction leads to off-center ignition of C flame, which moves inward but does not propagate to the center. This may form a hybrid C+O+Ne WD. These WDs can be a progenitor of the sub-classes of SNe Ia, called SNe Iax, which are expected preferably in dwarf galaxies (Kobayashi, Nomoto & Hachisu 2015; Cescutti & Kobayashi 2017). The nucleosynthesis yields of an SN Iax are taken from Fink *et al.* (2014).

Above this mass range, the off-center ignition of C flame moves inward all the way to the center ($\lesssim 9M_{\odot}$), or stars undergo central carbon ignition ($\gtrsim 9M_{\odot}$). For both cases, a strongly degenerate O+Ne+Mg core is formed (O+Ne dominant, but Mg is essential for electron capture). If the stellar envelope is lost by winds or binary interaction, an O+Ne+Mg WD may be formed. This upper mass limit is defined as the minimum mass for the Ne ignition, $M_{\rm up,Ne} \sim 9 \pm 1M_{\odot}$, and is smaller for lower metallicities.

$M_{\rm up,Ne} < M < 10M_{\odot}$ stars may have cores as massive as $\gtrsim 1.35M_{\odot}$ and ignite Ne off-centre. If Ne burning is not ignited at the centre (N13), or if off-center Ne burning does not propagate to the center (Jones *et al.* 2014), such a core eventually undergoes an electron-capture-induced collapse. This is the case for the Crab Nebula, and the

https://doi.org/10.1017/S1743921318007184 Published online by Cambridge University Press

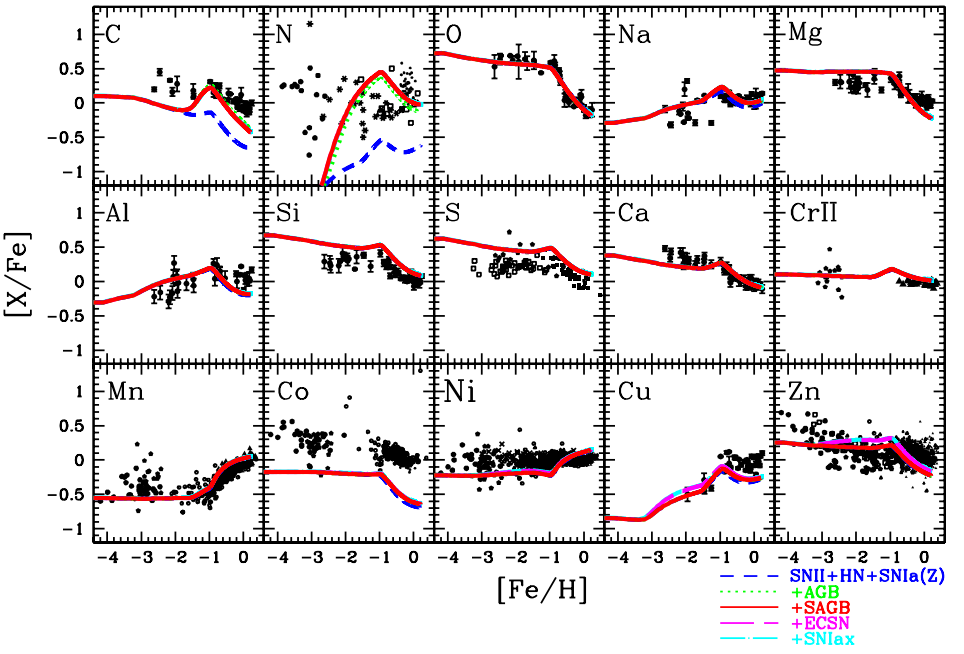

Figure 1. Evolution of elemental abundance ratios [X/Fe] against [Fe/H] in the solar neighborhood for the models with only supernovae (short-dashed lines), with AGB star (dotted lines), with super-AGB stars (solid lines), with ECSNe (long-dashed lines), and with SNe Iax (dot-dashed lines). See Kobayashi, Karakas & Lugaro (2018) for the observational data sources.

electron-capture supernova (ECSN) was one of the candidates of rapid neutron-capture process (r-process). The nucleosynthesis yields of an ECSN are taken from Wanajo *et al.* (2013).

In this paper, nucleosynthesis yields of super AGB stars and the mass ranges of the C+O+Ne WDs, O+Ne+Mg WDs, and ECSNe are taken from Doherty *et al.* (2015). Note that the Ne burning is not followed in Doherty *et al.* (2015); the lower-limit of ECSNe is defined with the temperature $\sim 1.2 \times 10^9$ K, and the upper limit is defined with the core mass $= 1.375 M_\odot$ at the end of carbon burning. These may underestimate the ECSN rate. We also note that these mass ranges are highly affected by convective overshooting, mass-loss, and reaction rates, as well as binary effects, and some of the important physics, such as the URCA process (Jones *et al.* 2014), are also not included. There is no region where the core mass is larger than the Chandrasekhar mass limit in the models compared in Doherty *et al.* (2015); if there were, the stars could explode as so-called Type 1.5 SNe, although no signature of such supernovae has yet been observed (Kobayashi *et al.* 2006).

Figure 1 shows the evolution of elemental abundance ratios [X/Fe] against [Fe/H] in the solar neighbourhood. The contribution to GCE from AGB stars (dotted lines) can be seen mainly for C and N, and slightly for Na. Hence, it would not be easy to explain the observed O-Na anti-correlation with a smooth star formation history as in the solar neighborhood. Although AGB stars produce significant amounts of Mg isotopes (K11), the inclusion of these do not affect the [Mg/Fe]-[Fe/H] relation. The contribution from super-AGB stars (solid lines) are very small; with super AGB stars, C abundances slightly decrease, while N abundances slightly increase. It would be very difficult to put a constraint on super-AGB stars from the evolutionary trends of elemental abundance ratios, but it might be possible see some signatures of super-AGB stars in the scatters

https://doi.org/10.1017/S1743921318007184 Published online by Cambridge University Press

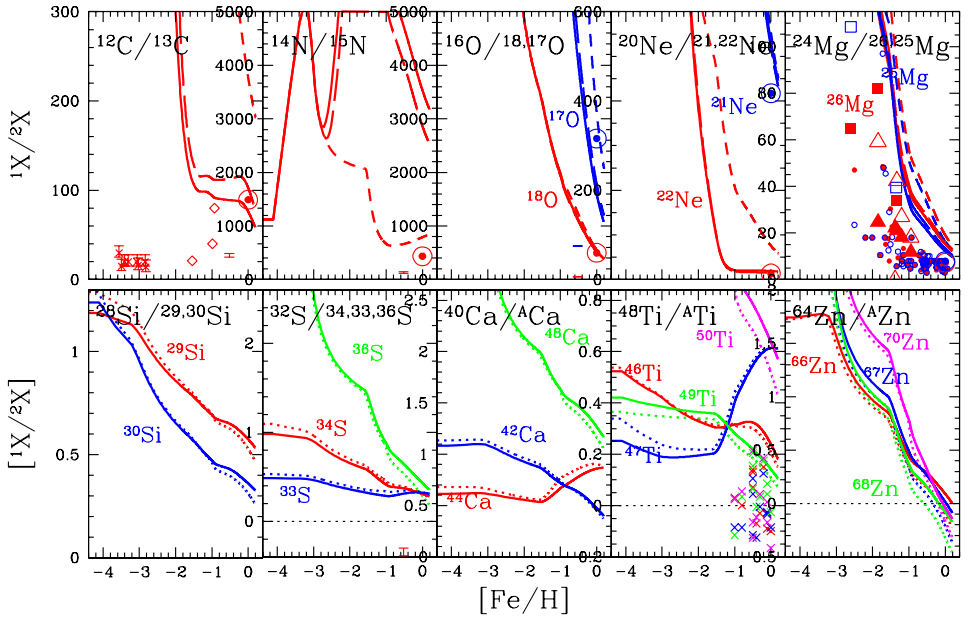

Figure 2. Evolution of isotope ratios against [Fe/H] for the solar neighborhood models: in the upper panels, the models without AGB/super-AGB stars (short-dashed lines), with AGB stars (long-dashed lines), and with super-AGB stars (the fiducial model, solid lines); in the lower panels, the fiducial model (solid lines), and the model without failed SNe (dotted lines). See Kobayashi, Karakas & Lugaro (2018) for the observational data sources.

of elemental abundance ratios. With ECSNe (long-dashed lines), Ni, Cu and Zn may be slightly increased. This is consistent with the high Ni/Fe ratio in the Crab Nebula (N13). Note that the nucleosynthesis yields of ECSNe may be different with neutrino oscillations (Pllumbi *et al.* 2015). No difference is seen with/without SNe Iax (dot-dashed lines) in the solar neighborhood because of the narrow mass range of hybrid WDs. Even with a wider mass range ($\Delta M \sim 1 M_{\odot}$ in Kobayashi, Nomoto & Hachisu 2015), however, the SN Iax contribution is negligible in the solar neighborhood, but can be important at lower metallicities such as in dwarf spheroidal galaxies with stochastic chemical enrichment (Cescutti & Kobayashi 2017).

Figure 2 shows the evolution of isotopic ratios against [Fe/H] for the solar neighborhood models with AGB and super-AGB stars (the fiducial model, solid lines), without super-AGB stars (long-dashed lines), without AGB nor super-AGB stars (short-dashed lines), and without failed SNe (dotted lines). The under-production problem of ^{15}N is known, and may require other sources such as novae (K11). ^{12}C/^{13}C, ^{16}O/^{17}O, ^{20}Ne/^{21}Ne, and ^{24}Mg/^{25,26}Mg ratios become smaller with AGB stars, and even smaller with super-AGB stars, while ^{14}N/^{15}N ratios become larger and larger. With super-AGB stars, ^{12}C/^{13}C is 76.2 at [Fe/H] $=0$ dex, which is lower than the solar ratio of 89.4. ^{17}O is too much produced in AGB and super-AGB stars. Even with super-AGB stars, however, ^{20}Ne/^{21}Ne and ^{24}Mg/^{25,26}Mg are larger than observations. There is no significant difference for ^{16}O/^{18}O and ^{20}Ne/^{22}Ne ratios, and these are determined from SN II/HN yields. Also for the elements heavier than Mg, the isotopic ratios mostly depend on SN II/HN yields, and the small mismatches for the solar ratios still remain.

Figure 3 shows the evolution of neutron-capture elements in the solar neighborhood. As shown for O, there are no differences for the elements up to Ni among these models.

https://doi.org/10.1017/S1743921318007184 Published online by Cambridge University Press

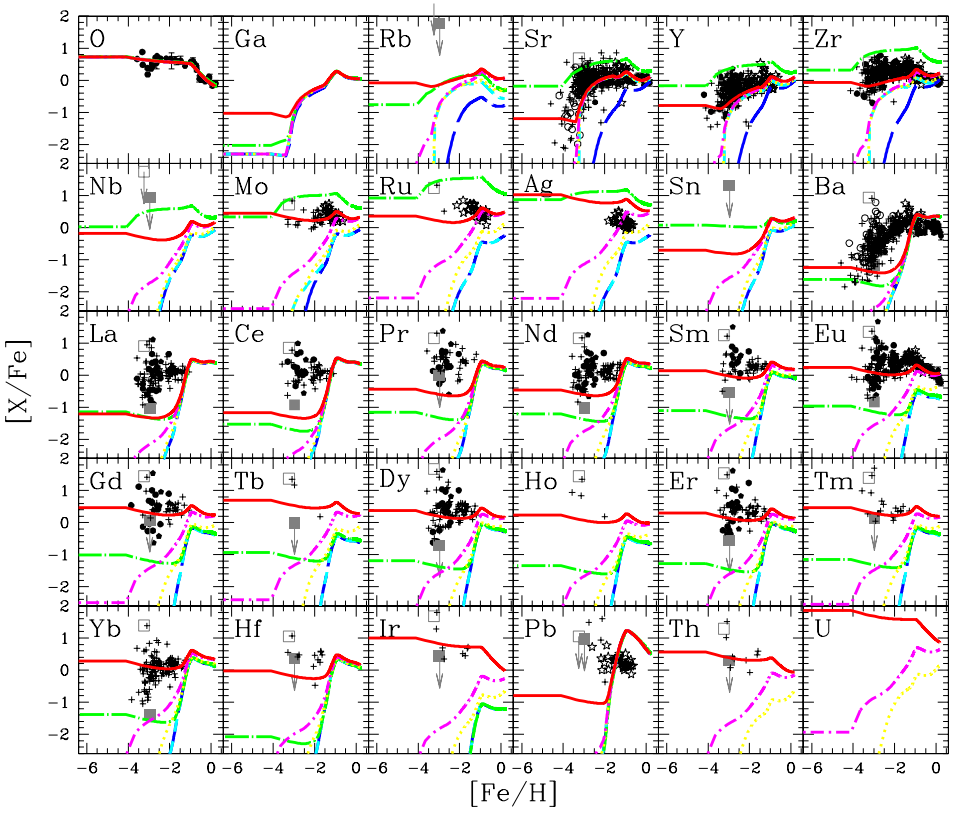

Figure 3. Evolution of the neutron-capture elemental abundances [X/Fe] against [Fe/H] in the solar neighborhood for the models with the s-process from AGB stars only (long-dashed lines) with ECSNe (short-dashed lines), with ECSNe and ν-driven winds (dot-long-dashed lines), with ECSNe and NS-NS mergers (dotted lines), with ECSNe and NS-NS/NS-BH mergers (dot-short-dashed lines), and with ECSNe, NS-NS/NS-BH mergers, and MRSNe (solid lines). See Kobayashi, Karakas & Lugaro (2018) for the observational data sources.

As predicted from nucleosynthesis yields, AGB stars (long-dashed lines) can produce more than enough s-process elements, such as Ba, Hf, and Pb. The contribution appears from [Fe/H] ~ -2 dex for light s-process elements (e.g., Sr, Y, Zr) and only from [Fe/H] ~ -1.5 dex for heavy s-process elements (e.g., Pb). With ECSNe (short-dashed lines), the enhancement is as small as ~ 0.1 dex for [(Cu,Zn)/Fe] (Fig. 1), but a larger enhancement is seen for Rb, Sr, Y, and Zr from [Fe/H] ~ -3 dex, which is enough together with AGB stars. With ν-driven winds (NUW, dot-long-dashed lines), the elements from Sr to Ag are over-produced, which is a crucial problem. The contribution can appear at [Fe/H] $<< -3$ dex, which may explain some of the observation at [Fe/H] $\lesssim -3$ dex, but the ratios between light and heavy neutron-capture elements are not consistent with observations. Therefore, it is better not to include ν-driven winds at all in GCE. With NS-NS mergers (dotted lines), the elements heavier than Mo show a small excess at [Fe/H] ~ -2 dex. The time-delay is shorter for NS-blackhole (BH) mergers (dot-short-dashed lines), and a larger excess is seen at [Fe/H] ~ -4 dex. However, this is still not short enough to explain the observations at [Fe/H] $\lesssim -3$ dex. Finally, with magneto-rotational supernovae (MRSNe, solid lines), it is possible to reproduce the plateau at [Fe/H] $\lesssim -3$ dex for most neutron-capture elements. Although these one-zone models

https://doi.org/10.1017/S1743921318007184 Published online by Cambridge University Press

cannot put a strong constraint on the site at [Fe/H] $\lesssim -2.5$ dex, it is better to include both NS-NS/NS-BH mergers and MRSNe in GCE.

3. Chemodynamical Simulations of Milky Way

In a real galaxy, the star formation history is not so simple and in particular the interstellar medium (ISM) is not homogeneous at any time, which is different from one-zone chemical evolution models. The effects of inhomogeneous enrichment can be summarized as follows. i) There is a local variation in star formation and metal flow by the inflow and outflow of the ISM. ii) Heavy elements are distributed via stellar winds and supernovae, and the elemental abundance ratios depend on the mass and metallicity of progenitor stars. iii) There is a mixing of stars due to dynamical effects such as merging and migration. All of these effects are, in principle, included in our chemodynamical simulation, where hydrodynamics, star formation, supernova feedback, and chemical enrichment are solved self-consistently throughout the galaxy formation. Note that the ISM may be mixed before the next star formation by other effects such as diffusion and turbulence, which might be underestimated (see Kobayashi 2014 for more details).

Using a chemo-hydro-dynamical code, Kobayashi & Nakasato (2011) succeeded in reproducing not only the observed trends but also the scatters of elemental abundance ratios from O to Zn. Under the inhomogeneous enrichment, there is only a weak age-metallicity relation of stars. In other words, the most metal-poor stars are not always the oldest stars. Therefore, the contribution of long-lifetime sources such as AGB stars can appear at low metallicities at a later epoch. In order to discuss the role of AGB stars, it is necessary to use a model that can treat inhomogeneous chemical enrichment, such as in our chemodynamical simulations.

In Haynes & Kobayashi (2018, hereafter HK18), we present the distributions of elemental abundance ratios using our chemodynamical simulations of a Milky Way-type galaxy. The code is based on the smoothed particle hydrodynamics (SPH) code GADGET-3, and include all relevant baryon physics (Kobayashi *et al.* 2007). We utilise cosmological zoom-in initial conditions for a Milky Way-type galaxy from the Aquila comparison project (Scannapieco *et al.* 2012) with cosmological parameters as follows: $H_0 = 100h = 73$ km s^{-1} Mpc^{-1}, $\Omega_0 = 0.25, \Omega_\Lambda = 0.75, \Omega_B = 0.04$. The initial mass of each gas particle is $3.5 \times 10^6 M_\odot$ and the gravitational softening length is $1h^{-1}$ kpc. We choose these conditions because they give a galaxy with morphology, size and merger history reasonably similar to the Milky Way (see the G3-CK model in Scannapieco *et al.* 2012). We also include the following sites of the r-process:

ECSNe: We adopt yields from Wanajo *et al.* (2013) for a $8.8 M_\odot$ star and metallicity dependent ($\log Z = -4, -3, -2.4, -2.1, -1.7$) limits of the progenitor mass with the upper (8.4, 8.4, 9.0, 9.65, 9.9 $M_\odot$) and lower (8.2, 8.25, 8.8, 9.5, 9.75 $M_\odot$) bounds (Doherty *et al.* 2015). For metallicities above or below the limits, we assume the rates derived from the upper and lower limits, respectively.

NUW: Ejecta heated by neutrinos from proto-neutron stars (NSs) can provide a site for r-process enrichment. The yields are taken from Wanajo (2013) for stars between 13 and 40 $M_\odot$ with a conversion between the stellar masses (13, 15, 20, 40) $M_\odot$ and the respective NS masses (1.4, 1.6, 1.8, 2.0) $M_\odot$.

NS Mergers: NS mergers provide a site for the r-process in the neutron rich dynamic ejecta created as the binary system merges. We include yield tables for NS-NS mergers (both 1.3 $M_\odot$) from Wanajo *et al.* (2014) and for NS-BH mergers. The NS-NS merger and NS-BH merger rates of simple stellar populations are taken from the binary population synthesis calculations in Mennekens & Vanbeveren (2014) (model 2 for $Z = 0.02$

https://doi.org/10.1017/S1743921318007184 Published online by Cambridge University Press

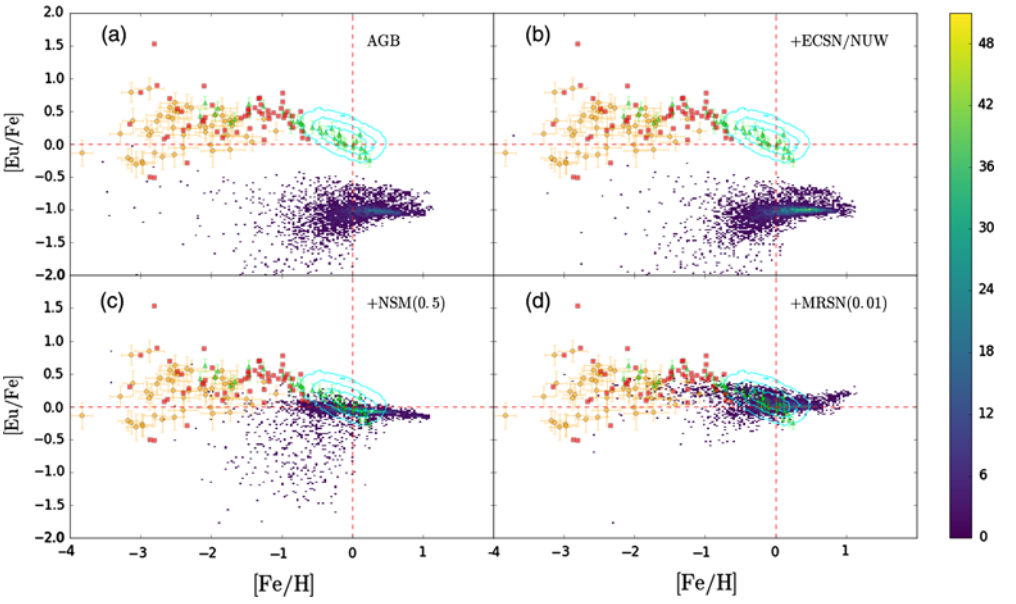

Figure 4. [Eu/Fe] plotted against [Fe/H] for the star particles in the solar neighborhood in our Milky Way simulations at $z = 0$. The panels in order show: supernovae+AGB only, with ECSNe and ν-driven winds, NSMs, and MRSNe. See HK18 for the observational data sources for high-resolution (red squares, green triangles, orange circles) and the HERMES-GALAH survey (cyan contours). The contours show 10, 50 and 100 stars per bin. The red dashed lines denote 0 for both [Eu/Fe] and [Fe/H] which we expect to lie within our data. The color bar shows the linear number of points per bin for our simulation.

and 0.002). We also introduce a free parameter, $f_{\rm NSM}$, representing the fraction of stars in binary systems in our simulations. We choose an initial value of $f_{\rm NSM} = 0.5$, independent of metallicity.

MRSNe: Rapidly rotating massive stars with strong magnetic fields may provide a potential site for r-process nucleosynthesis at the inner boundary of the accretion disc formed around the central collapsed object. We use the yield tables presented in Nishimura *et al.* (2015) for a 25 $M_\odot$ star (B11β1.00 model). This event could be related to HN events, which also require rotation and magnetic fields; recent simulations of supernova explosions have not succeeded in exploding very massive stars ($M \geqslant 25\ M_\odot$). Therefore, we replace a fraction of HN events with MRSNe. The number of stars with suitable conditions for MRSNe is poorly constrained so we introduce a free parameter, $f_{\rm MRSN}$, representing the fraction of stars with the correct conditions. Our initial value is $f_{\rm MRSN} = 0.01$, independent of mass and metallicity, as it gives solar values at [Fe/H]$= 0$ dex and reasonable agreement with observations.

Figure 4 shows the distribution of [Eu/Fe] against [Fe/H]. Panel (a) shows the control simulation with the AGB contributions but no additional r-process sites. The spread of [Eu/Fe] sits well below observational values; [Eu/Fe] is at ~ -1 for [Fe/H] $\gtrsim -1.5$ dex. Panel (b) shows the addition of both NUW and ECSNe to the AGB model. The addition is insufficient to boost [Eu/Fe] to the observed levels and the overall trend remains at [Eu/Fe] ~ -1. This is expected from the input yields: no Eu enrichment from ECSNe and only a small contribution from NUW. Panels (c) and (d) show simulations using NSMs and MRSNe, respectively. Both NSMs and MRSNe increase [Eu/Fe] to ~ 0 at [Fe/H] $= 0$ dex, though with the caveat that both make use of a free parameter that allows the level to be adjusted reasonably freely in our simulations.

https://doi.org/10.1017/S1743921318007184 Published online by Cambridge University Press

At [Fe/H] $\lesssim -1.5$ dex the simulated level and scatter of [Eu/Fe] in the MRSN model matches the observational data much better than the NSM model. This is a result of delay times before NSMs can occur, as NS binaries need to both form and coalesce. MRSNe, on the other hand, are assumed to be a subset of 25–40 $M_\odot$ HNe in our simulations and able to start producing r-process elements almost immediately after the formation of stars. Additionally, the NSM model displays a large amount of scatter below the main trend of at [Fe/H] $\lesssim 0$ dex. We already see a similar scatter at the same [Fe/H] range in the control simulation; the scatter we see in NSMs is likely produced by AGB stars. However, this same pattern of scatter is not present in the MRSN model. In this case it appears that the production of Eu from NSMs is too slow to raise [Eu/Fe] to observed levels at [Fe/H] < -1 dex and instead slowly increases [Eu/Fe] between $-2 \lesssim$ [Fe/H] $\lesssim 0$ dex. However, MRSNe are able to enrich the ISM prior to AGB contributions so no such scatter is seen. Although MRSNe replicate the trend in this region substantially better, it presents a flat trend above [Fe/H] ~ -1 dex where the observational data suggests a downward trend. NSMs have a slight downward trend in this region, though not as steep as the observed data. Both the scatter and average [Eu/Fe] are important for constraining the r-process. SNe Ia produce substantial amounts of Fe which contributes to the scatter in Figure 4, so in order to remove the SN Ia contribution, we also show the [Eu/O] distributions in HK18, and reach the same conclusion as from [Eu/Fe].

4. Cosmological Simulations

On a cosmological scale, chemical enrichment takes place even more dramatically (see a movie by Philip Taylor, https://www.youtube.com/watch?v=jk5bLrVI8Tw). There is gas accretion along the cosmological filaments, where star formation and chemical enrichment are already occurring. This results in strong supernova-driven winds because of the shallow potential in the filaments. As the central galaxy grows through the accretion, a super-massive blackhole also grows (following the so-called M–σ relation), which eventually causes even stronger winds driven by the active galactic nuclei. Metallicity is very spatially inhomogeneous; the center of massive galaxies can reach super-solar metallicity at high redshifts, while the accreted component has only one-hundredth of solar metallicity as it is mainly fed from the intergalactic medium. The wind component has about one-tenth of solar metallicity as it is a mixture of the inflow gas and supernova ejecta. This simulation successfully reproduces various observations of galaxies including the mass-metallicity relation of galaxies (massive galaxies are more metal-rich, Taylor & Kobayashi 2015).

In Vincenzo & Kobayashi (2018b, hereafter VK18b), from another cosmological simulation (with side 10 h^{-1} Mpc) we create a catalogue of 33 stellar systems at redshift $z = 0$, all embedded within dark matter (DM) halos with virial masses in the range $10^{11} \leqslant M_{\rm DM} \leqslant 10^{13} M_\odot$. The mass and spacial resolutions of gas are $6.09 \times 10^6\, h^{-1} M_\odot$ and $0.84\, h^{-1}$ kpc, respectively. Within a galaxy, the metallicity distribution is not uniform either, and the central parts of the galaxies are more metal-rich than the outskirts of the galaxies. This metallicity radial gradient evolves as a function of time. In disk galaxies, the metallicity gradients become steeper at higher redshifts because of inside-out formation of discs (Vincenzo & Kobayashi 2019).

Using our cosmological hydrodynamical simulation, we succeed in reproducing the observed N/O–O/H relation. The observed increasing trend of N/O at high O/H in the individual ISM regions of spatially resolved star-forming disc galaxies (we refer to it as local N/O–O/H relation) can be explained as the consequence of metallicity gradients that have settled in the galaxy ISM, where the innermost regions possess both the highest O/H and the highest N/O ratios (see Fig. 4 of VK18b).

https://doi.org/10.1017/S1743921318007184 Published online by Cambridge University Press

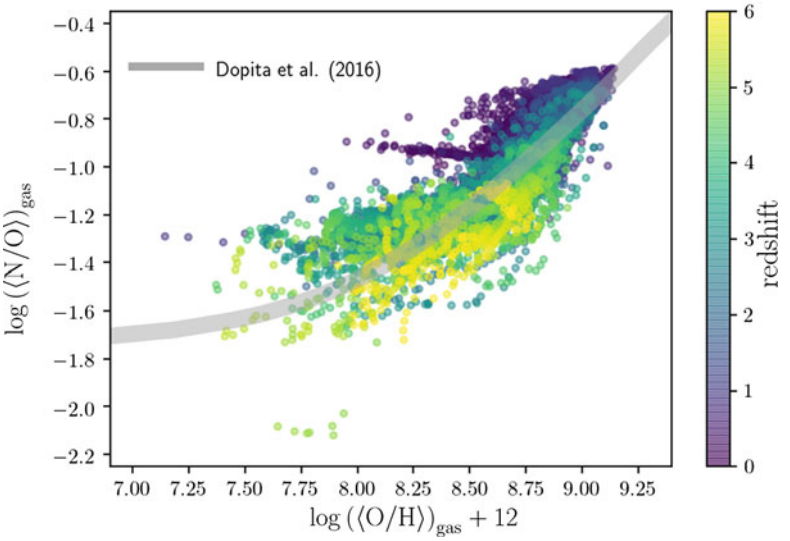

Figure 5. The redshift evolutionary tracks of 33 galaxies from our cosmological simulation in the O/H–N/O diagram. The abundances in the figure correspond to SFR-weighted averages in the gas-phase of the ISM. The color coding represents the redshift. See VK18b for the observational data source (grey bar).

Similar relation is known for average abundances from the whole galaxy ISM. Figure 5 shows the star formation rate (SFR)-weighted averages in the gas-phase of the ISM of 33 galaxies in our catalogue. This global N/O–O/H relation is the consequence of an underlying mass–metallicity relation that galaxies obey as they evolve across the cosmic epochs. In this case, the predicted N/O–O/H relation is an average evolutionary trend that is followed by the chemical evolution tracks of all galaxies at almost any redshift.

Our simulation predicts an almost flat trend of N/O versus O/H at high redshifts, which is caused by an inhomogeneous enrichment of the galaxy ISM with a significant contribution of AGB stars at low metallicity. Our simulation represents an improvement with respect to previous chemical evolution models, both because the N/O–O/H relation was studied with simple one-zone models with instantaneous mixing approximation and because we did not assume any artificial primary N production by massive stars. We note that the N/O plateau would be too high if rapidly rotating massive stars were included.

We then predict how the C, N, and O abundances within the interstellar medium of galaxies evolve as functions of the galaxy star formation history (SFH). In Vincenzo & Kobayashi (2018a, hereafter VK18a), we focus on three star-forming disc galaxies (Galaxy A, B, and C) with different SFHs in our cosmological simulation (left panels of Fig. 6). At the beginning of galaxy formation, CNO are produced by core-collapse supernovae, N is enhanced by intermediate mass AGB stars ($\gtrsim 4M_{\odot}$), then C is enhanced by low-mass AGB stars ($\lesssim 4M_{\odot}$). In the right panels of Figure 6, we predict that the average N/O and C/O steadily increase as functions of time, while the average C/N decreases, due to the mass and metallicity dependence of the yields of AGB stars; such variations are more marked during more intense star formation episodes. Our predictions on the CNO abundance evolution can be used to study the SFH of disc galaxies with the *James Webb Space Telescope*.

https://doi.org/10.1017/S1743921318007184 Published online by Cambridge University Press

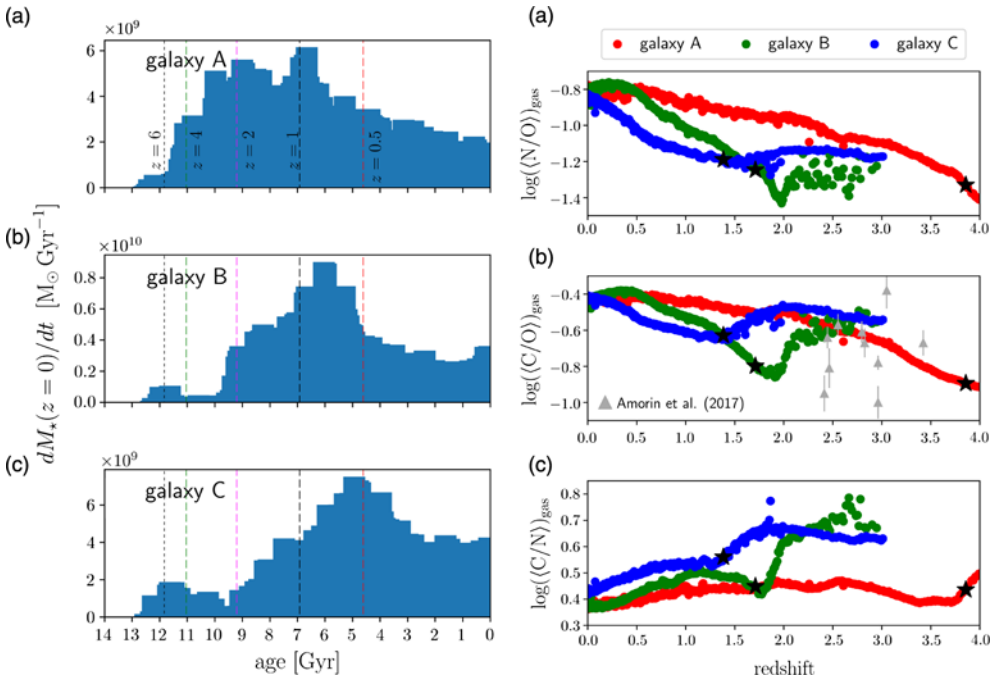

Figure 6. (a) Distribution of the present-day total stellar mass as a function of the star particle age. (b) Average SFR-weighted gas-phase log (N/O), log (C/O) and log (C/N) as functions of redshift. We only show the predictions of our simulation for the redshifts when the galaxy stellar mass $M_* \geqslant 10^8 M_\odot$. The black star symbol on each track marks the redshift when $M_* \simeq 10^9 M_\odot$. See VK18a for the observational data source (grey triangles with the error bars).

References

Carlos, M., Karakas, A. I., Cohen, J. G., Kobayashi, C., & Meléndez, J. 2018, *ApJ*, 856, 161
Cescutti, G., & Kobayashi, C. 2017, *A&A*, 607, 23
Doherty, C. L., Gil-Pons P., Siess L., Lattanzio J. C., & Lau H. H. B., 2015, *MNRAS*, 446, 2599
Fink, M., *et al.* 2014, *MNRAS*, 438, 1762
Haynes, C., & Kobayashi, C. 2018, *MNRAS*, submitted arXiv:1809.10991 (HK18)
Jones, S. Hirschi, R., & Nomoto, K. 2014, *ApJ*, 797, 83
Karakas, A. I., & Lugaro, M., 2016, *ApJ*, 825, 26
Kobayashi, C. 2014, IAU S298, 167
Kobayashi, C. 2016, *Nature*, 540, 205
Kobayashi, C., Izutani, N., Karakas, A. I., *et al.*, 2011a, *ApJ* (Letters), 739, L57
Kobayashi, C., Karakas, I. A., & Lugaro, M. 2018, in preparation
Kobayashi, C., Karakas, I. A., & Umeda, H. 2011b, *MNRAS*, 414, 3231 (K11)
Kobayashi, C., & Nakasato, N. 2011, *ApJ*, 729, 16
Kobayashi, C., & Nomoto, K. 2009, *ApJ*, 707, 1466
Kobayashi, C., Nomoto, K., & Hachisu, I. 2015, *ApJ* (Letters), 804, L24
Kobayashi, C., Springel, V, & White, S. D. M. 2007, *MNRAS*, 376, 1465
Kobayashi, C., Tsujimoto, T., & Nomoto, K. 2000, *ApJ*, 539, 26
Kobayashi, C., Umeda, H., Nomoto, K., Tominaga, N., & Ohkubo, T. 2006, *ApJ*, 653, 1145
Mennekens N., & Vanbeveren D. 2014, *A&A*, 564, A134
Nishimura, N., Takiwaki, T., & Thielemann, F.-K. 2015, *ApJ*, 810, 109
Nomoto, K., Kobayashi, C., & Tominaga, N. 2013, *ARAA*, 51, 457 (N13)
Pllumbi, E., Tamborra, I., Wanajo, S., Janka, H.-T., & Hüdepohl, L. 2015, *ApJ*, 808, 188
Scannapieco, C. *et al.* 2012, *MNRAS*, 423, 1726
Taylor, P., & Kobayashi, C. 2015, *MNRAS*, 448, 1835

https://doi.org/10.1017/S1743921318007184 Published online by Cambridge University Press

Vincenzo, F., & Kobayashi, C. 2018a, *A&A*, 610, L16 (VK18a)
Vincenzo, F., & Kobayashi, C. 2018b, *MNRAS*, 478, 155 (VK18b)
Vincenzo, F., & Kobayashi, C. 2019, IAU FM7, in press
Wanajo, S., 2013, *ApJ* (Letters), 770, L22
Wanajo, S., Janka, H.-T., & Müller, B., 2013, *ApJ* (Letters), 767, L26
Wanajo, S., Sekiguchi, Y., Nishimura, *et al.* 2014, *ApJ* (Letters), 789, L39

Discussion

VENTURA: One of the open points in AGB modelling is the extent of oxygen destruction in massive AGB stars. Is there any possibility of investigating this issue in the context of your modelling?

KOBAYASHI: Most of O is produced from core-collapse SNe, and the signature of oxygen destruction will be washed out in the averaged evolution. However, it may be possible to see some differences in the scatter of N/O ratios.

DE MARCO: Is there a way you can constrain delay-times for SNe (from Fe) or NS-NS mergers (from r-process elements)?

KOBAYASHI: This is done for SNe Ia. For example, binary population synthesis models give too short delay times for double degenerate, which cannot reproduce the sharp decrease of [α/Fe] from [Fe/H] $\sim$ -1 (Kobayashi & Nomoto 2009). For NSMs, it is not so straightforward as r-process elements can be produced by other sources. The community is working on that and it will be possible in the future.

SAHAI: Is it important to consider and analyze the $^{13}C/^{12}C$ enrichment, say as a function of Z, since we know that AGBs definitely can increase $^{13}C/^{12}C$ in ISM of galaxies?

KOBAYASHI: Yes, very much. $^{13}C/^{12}C$ vary as well as C/N, and it should also be possible to measure with ALMA. There are some measurements at $Z = 0$ already, but the available values do not make sense and maybe are still too uncertain.

https://doi.org/10.1017/S1743921318007184 Published online by Cambridge University Press